

**USING EUV IMAGE SEQUENCES TO  
QUANTIFY MAGNETIC RECONNECTION  
IN THE SOLAR CORONA**

**PROJECT SUMMARY**

Magnetic reconnection is a process, universal in astrophysical plasmas, that both topologically changes magnetic field lines and converts magnetic energy into other forms of energy such as heat and bulk kinetic energy. Theoretical models of reconnection predict a relationship between the rates at which these two distinct effects occur. Owing to the difficulty of measuring the rate of topological field line change within a volume of plasma, this relationship has been subject to few observational tests or constraints. One such test was made by Longcope et al. (2005), using TRACE EUV images of an active region emerging and then reconnecting to a nearby, older active region. It was found that *reconnection did not occur at the same rate as it was driven*. Instead, a roughly 24 hour delay was observed between the emergence of the active region and its reconnection to the overlying coronal field. Unfortunately, the TRACE archive contained no other cases suitable for similar study so this remains an isolated measurement. We have improved on the methodology used in that seminal study and propose here to apply it to EUV sequences from SDO/AIA of active regions emerging in the neighborhood of existing regions. We will apply the improved methodology to 8–16 cases, already identified in the data archives. The energy conversion rate will be measured using DEMs constructed with images from SDO/AIA and from *Hinode*/XRT. These reconnection studies will allow us to answer fundamental questions concerning magnetic reconnection in the corona including the following. Is a delay between emergence and reconnection typical, and if so what is a typical delay? How much current accumulates in the corona prior to reconnection? Does the relationship between topological change and energy dissipation depend on the accumulated current as theoretical models predict? What is the distribution of elemental flux transfers (i.e. flux tubes) in the reconnection? Answering any of these would address a Research Focus Area of NASA’s 2009 Roadmap: “What are the fundamental physical processes and topologies of magnetic reconnection?”

COVER PAGE AND PROPOSAL SUMMARY

TABLE OF CONTENTS ..... i

SCIENTIFIC/TECHNICAL/MANAGEMENT

1. SCIENTIFIC OBJECTIVE & ITS SIGNIFICANCE ..... 1

2. TECHNICAL APPROACH & METHODOLOGY ..... 3

    Driving reconnection: Emergence ..... 3

    Reconnection: Flux transfer ..... 5

    Reconnection: Energy release ..... 7

3. PROPOSED WORK ..... 8

    Case selection ..... 9

    Flux transfer measurements ..... 10

    Magnetic Modeling ..... 10

    Energetics ..... 12

4. EXPECTED RESULTS & PERCEIVED IMPACT ..... 12

5. RELEVANCE TO NASA'S PROGRAMS ..... 14

6. PLAN OF WORK ..... 15

7. DATA SHARING PLAN ..... 15

REFERENCES ..... 16

FACILITIES AND EQUIPMENT ..... 19

CURRICULA VITAE ..... 20

CURRENT AND PENDING SUPPORT ..... 24

BUDGET & JUSTIFICATION ..... 27

    Summary of personnel & work efforts ..... 27

    Budget details ..... 28

# 1 Scientific Objective & Its Significance

The previous generation of NASA-supported Solar Physics missions, most notably *Yohkoh*, SoHO and TRACE, have been instrumental in firmly establishing magnetic reconnection as the primary driver of solar activity. For example cusp-shaped loops in solar flares are strongly suggestive of reconnected field lines, and the hot lobes along each side of the cusp—measured using the multiple filters of the *Yohkoh* Soft X-ray Telescope (SXT)—support this interpretation in detail (Tsuneta, 1996).

In the earliest models, set in idealized two-dimensional geometries (Parker, 1957; Sweet, 1958; Petschek, 1964; Sonnerup, 1970; Vasyliunas, 1975), the process of magnetic reconnection produced two distinct effects: 1. a change in the topology of magnetic field lines, 2. a conversion of magnetic energy into heat and bulk kinetic energy. There has been a tendency in subsequent studies to use the term “magnetic reconnection” in reference to one of these effects or the other. Either effect may, however, occur by itself in the absence of true magnetic reconnection. For example, magnetic field may be annihilated at a current sheet to dissipate energy while producing little or no topological changes in exterior field lines. To understand the role played by genuine reconnection in driving coronal activity we must quantify both its effects and understand how they are related.

Energy deposition may be quantified, in principle, either by characterizing the thermodynamic properties of the heated plasma or the population of accelerated particles. It is a less straightforward task to quantify the topological changes the reconnection produces in the coronal field. This is the primary contribution made by the novel methodology underpinning the work proposed here. Making this measurement puts us in the unique position of seeing both aspects of reconnection, flux transfer *and* energy release, for the same plasma. It is then possible to test or constrain the relationship predicted by the original reconnection models.

Coronal images in EUV or soft X-ray passbands provide the best tracers of topology since they show plasma outlining coronal magnetic field. Supplementing the topological determination with a measurement of magnetic flux yields a reconnection flux transfer rate. We have performed such a measurement in one instance, and propose here to apply this method to a large amount of new data from SDO and *Hinode*/XRT.

The method we have developed requires field line topology to be routinely and unambiguously determined from coronal images. The resolution of the present magnetograms (SDO/HMI) and imagery (SDO/AIA and *Hinode*/XRT) requires us to look for reconnection between clearly distinguished photospheric flux sources. One of the easiest distinctions to make, even with magnetograms of modest resolution, is between polarities of different active regions. We therefore focus our study on reconnection between different active regions (ARs).

Our method uses the emergence of a new AR in the vicinity of an older (existing) AR to quantify reconnection flux transfer. Prior to emergence an AR’s magnetic field is thought to be confined to a flux tube. Where the flux tube crosses the photosphere it creates two photospheric polarities. At the instant of emergence all coronal field lines from one polarity will connect only to its counterpart. Any field lines later observed *interconnecting* the two ARs *must* have been forged by coronal reconnection. By tabulating the net flux found in interconnecting field we are quantifying the topological changes produced by reconnection.

This approach was applied in Longcope et al. (2005) to the emergence of NOAA AR9574 in the vicinity of AR9570 over a 41-hour period beginning on 2001-Aug-10, observed in 171Å by TRACE and with line-of-sight magnetograms by SoHO/MDI. We found that little reconnection occurred during the first 24 hours after emergence began. Following that delay we observed a burst of reconnection flux

transfer at rates as high as  $10^{17}$  Mx/sec (1 Gigavolt). This topological change was accompanied by an energy release of at least  $2.5 \times 10^{30}$  ergs over a period of about 3 hours brightening the interconnecting loops in soft X-rays.

This study made quantitative measurements of several aspects of magnetic reconnection in the solar corona—at least as it occurred on August 11, 2001. It is likely that these same features would be found in other reconnection-driven events such as flares or coronal mass ejections. Due to the ease of topological discrimination, however, reconnection between active regions is the ideal scenario to study the process quantitatively. It is essential to determine which of the conclusions drawn from the 9570/9574 case are general to all reconnection. We propose to do this by applying the same analysis method to 8–16 other emergences.

Under a previous SR&T award (NNX07AI01G 2007–2011) the proposing team improved significantly upon the methodology of Longcope et al. (2005) using more data from TRACE and SoHO/MDI. They developed an improved method of magnetic modeling that combined *both* the line-of-sight magnetogram data and the EUV imaging data (Malanushenko et al., 2009, 2011). (This method has been developed still further into a powerful, general tool by Malanushenko et al. (2012, 2014).) They also streamlined the flux-identification algorithm and searched TRACE and SoHO data for emerging/existing AR pairs to which it could be applied. Four potential cases were found, but in each case TRACE’s incomplete coverage or limited field of view compromised the data. We concluded that 9570/9754 was the best case TRACE observed during its operation.

The Solar Dynamics Observatory (SDO) has a full-Sun field of view, wider range of temperature sensitivity, and higher imaging cadence compared to TRACE, making it ideal for detecting and identifying the AR/AR reconnections. *Hinode*/XRT offers enhanced spatial resolution compared to *Yohkoh*/SXT and a view of the Sun uninterrupted by orbital eclipses like those experienced year-round by *Yohkoh*, thereby permitting the XRT data to be much more effective at supporting measurements for plasma conditions in the interconnecting loops. The objective of this new proposal is to apply our powerful techniques, for the first time, to SDO data in order to obtain time-resolved measurements of reconnection between ARs for a significant number of cases. We will also use SDO/AIA and *Hinode*/XRT data to quantify the energy released by the magnetic reconnection. **The science goal of this investigation is to address observationally five questions concerning the fundamental process of magnetic reconnection and its occurrence in the solar corona.**

- Q1: How does the rate of reconnection compare to the rate of its driving from the photosphere? Is the kind of delay observed in AR 9574 typical? If so, what is the length of the typical delay prior to reconnection?
- Q2: How much coronal current builds up before reconnection? Can the current, its attendant free energy or magnetic helicity, be identified as the threshold triggering the onset of reconnection?
- Q3: What is the relationship between *topological* change (i.e. the rate  $\dot{\Phi}$  at which interconnecting field lines are created) and *energy release* (i.e. power  $P$ )? If the two rates are proportional then the constant of proportionality,  $P/\dot{\Phi}$ , has units of current (Tarr et al., 2014). Does this value match or even scale with the current from Q2?
- Q4: What range of reconnection electric fields is observed in these reconnection events? Is the electric field related to the current in Q2 or the delay in Q1?
- Q5: What is the distribution of flux tube diameters (and fluxes) created by the reconnection process? Does this vary between different events or is it a fundamental characteristic of coronal reconnection? How does this relate to the value of the reconnection electric field from Q4?

## 2 Technical Approach & Methodology

Our proposed reconnection study uses a time-sequence of magnetograms to characterize the emergence of one AR into a coronal field established by a neighboring AR. The analysis proceeds as follows. Photospheric magnetograms characterize the emergence directly, and are extrapolated to characterize the field within the corona where the two regions interact. A sequence of X-ray or EUV images are then used to identify coronal loops whose flux interconnects new and old photospheric polarities; these loops trace field which is necessarily *reconnected flux*. The coronal extrapolation is used to assign a magnetic flux to each interconnecting loop thereby providing a measurement of the rate,  $\dot{\Phi}(t)$ , at which magnetic flux is being topologically changed, i.e. reconnected. Finally, the properties of the plasma within the volume of reconnected flux are characterized using EUV and Soft X-ray images. This provides a measurement of the energy release rate,  $P$ , which accompanies the topological change. **The goal of any reconnection model must be to explain the relationship between topological change and energy release in the form of a mathematical relation between  $\dot{\Phi}$  and  $P$ . Our investigation will provide observational constraints on that relationship.**

In the following we elaborate on each step in this methodology. We illustrate them using the study of Longcope et al. (2005) which remains the single case where the method has been most completely applied. We also draw on subsequent studies to illustrate the improvements we have made, and intend to apply to new emergence studies.

### 2.1 Driving reconnection: Emergence

The coronal reconnection we observe is clearly driven from the photosphere by the emergence of new polarities into an existing coronal field. The first step in the analysis is to characterize this driving using a sequence of magnetograms spanning the entire emergence period, typically two days or more. A modest magnetogram cadence, as low as 120 minutes, has proven adequate for capturing this fairly slow driving process. Figure 1 shows three of the 96-minute line-of-sight magnetograms from SoHO/MDI, used to characterize the emergence of AR9574 in the neighborhood of AR9570.

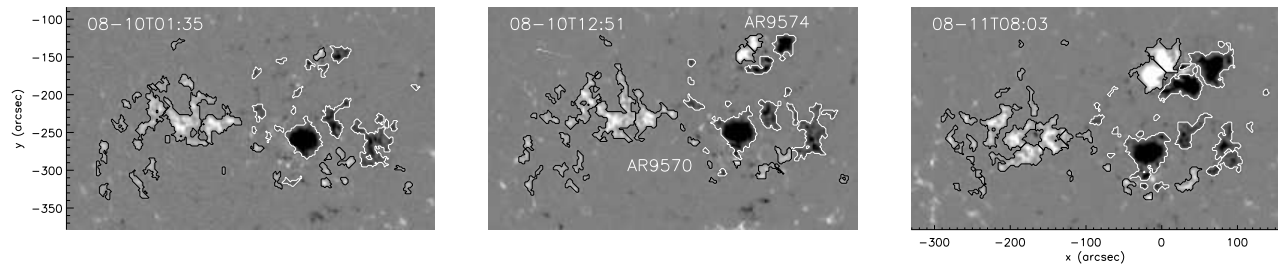


Figure 1. MDI magnetograms (gray scale) of AR 9574 emerging in the neighborhood of existing region 9750 over Aug. 10 and 11, 2001, partitioned into contiguous source regions (outlined).

The salient feature of the photospheric field is its concentration into new (emerging) and old (previously emerged) polarities. We use an automated algorithm to group magnetogram pixels into polarity concentrations (Barnes et al., 2005). This algorithm groups contiguous pixels and can also break those contiguous regions into distinct sub-regions. We combine all the regions into four distinct polarities: old, called  $P1$  and  $N1$ , and newly emerging, called  $P2$  and  $N2$ . The fluxes found for 9570 (old) and 9574 (new) are plotted as broken and solid curves respectively in fig. 2. The old polarities,  $P1$  and  $N1$ , remain roughly constant,  $\Psi_1 \simeq 1.3 \times 10^{22}$  Mx, throughout, while each emerging polarity increases to  $\Psi_2 \simeq 1.1 \times 10^{22}$  Mx beginning at approximately 07:34 on 2001-Aug-10. Initially the emergence occurs at a fairly steady rate  $\dot{\Psi}_2 \sim 1.2 \times 10^{17}$  Mx/sec while the polarities separate at an approximately

constant speed of 215 m/sec. We point to the close match between the emergence of the two polarities (the signed fluxes, plotted in fig. 2, are very nearly zero for each bipole) as corroboration of the flux tube hypothesis.

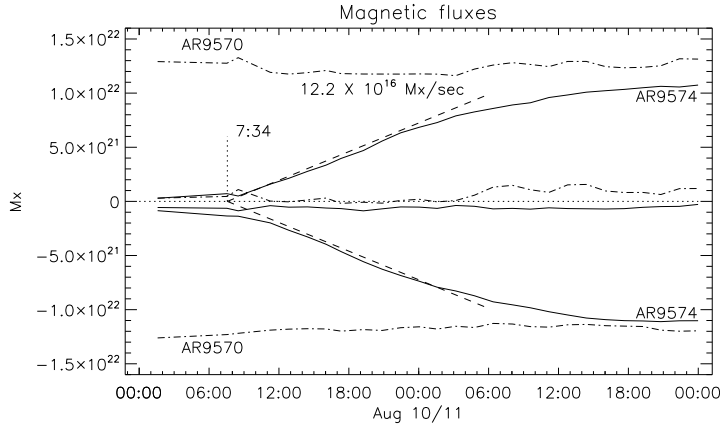


Figure 2. The fluxes in the old region (AR9570, broken) and new, emerging region (AR9574, solid) found from MDI magnetograms. The fluxes in the positive and negative polarities are plotted above and below the zero line (dotted). Their sum, the signed flux, is plotted between them. A linear fit to the emerging period of AR9574 is plotted as a pair of dashed lines.

While the actual coronal field will certainly differ from the potential field, the two will share a basic topology: four classes of field lines interconnecting the four photospheric concentrations. In any field of this topology a single separator traces out the place where all four domains come into contact. Magnetic reconnection occurs when topological changes increase flux in two domains, while decreasing the flux in the other two. It is necessary that this topological change occur at the separator. To remain in its potential state, topological change would need to proceed at the rate  $\dot{\Phi}_{21}^{(v)} \simeq 1.5 \times 10^{16}$  Mx/sec, determined from fig. 3. This would require an electromotive force (EMF) of

$$\mathcal{E}^{(v)} = \int \mathbf{E} \cdot d\mathbf{l} = 1.5 \times 10^8 \text{ Volts} \quad (1)$$

to be maintained along the single separator. The highly conducting coronal plasma precludes this electric field parallel to a field line. This leads to the build-up of current in the corona (i.e. the observed departure from a potential field) culminating, ultimately, in a period of reconnection during which a substantial electric field *is* supported along the

Before attempting to model the coronal field we obtain an upper bound on the interconnecting flux using a potential field extrapolation. Field lines traced in this extrapolation can be assigned to domains according to their footpoints. The set of field lines from one domain, for example connecting  $P2$  to  $N1$ , can be used in a Bayesian estimate of the net flux in that domain,  $\Phi_{21}^{(v)}$  (Barnes et al., 2005; Longcope et al., 2009a). While we do not assume the coronal field is actually current-free,  $\Phi_{21}^{(v)}$  provides a bound on the actual interconnecting flux  $\Phi_{21}$ , since the former is the state of minimum energy. In the case shown in fig. 3  $\Phi_{21}^{(v)}$  rises from zero to about  $1.9 \times 10^{21}$  Mx (about 16% of the total emerging flux,  $\Psi_2$ ) at a relatively steady rate of  $\dot{\Phi}_{21}^{(v)} \simeq 1.5 \times 10^{16}$  Mx/sec.

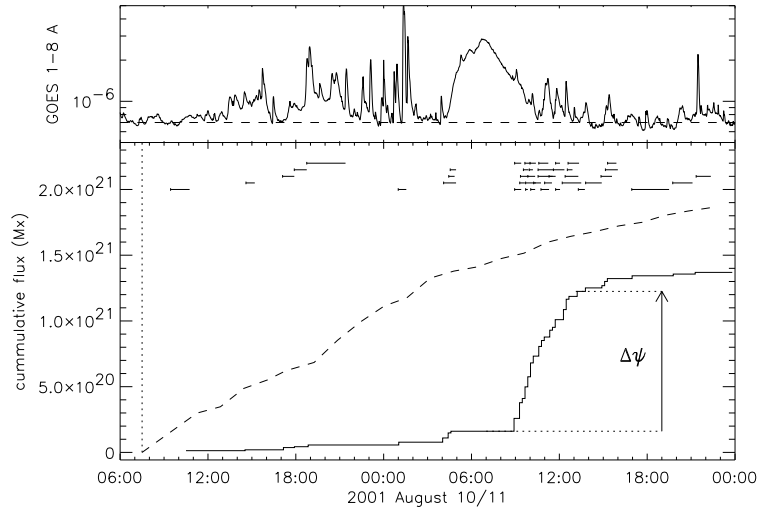


Figure 3. The time history of the interconnecting flux. *Bottom* panel shows the interconnecting flux (in Maxwells) of the potential model (dashed). Horizontal bars along the top show the lifetimes of each of the 43 interconnecting loops found in TRACE 171Å images. The fluxes inferred from these loops are accumulated to form the solid “staircase” curve representing the actual interconnecting flux. *Top* panel is the 1-8Å channel of GOES.

separator, but within a large current density (i.e. a current sheet).

## 2.2 Reconnection: Flux transfer

### 2.2.1 The coronal magnetic field

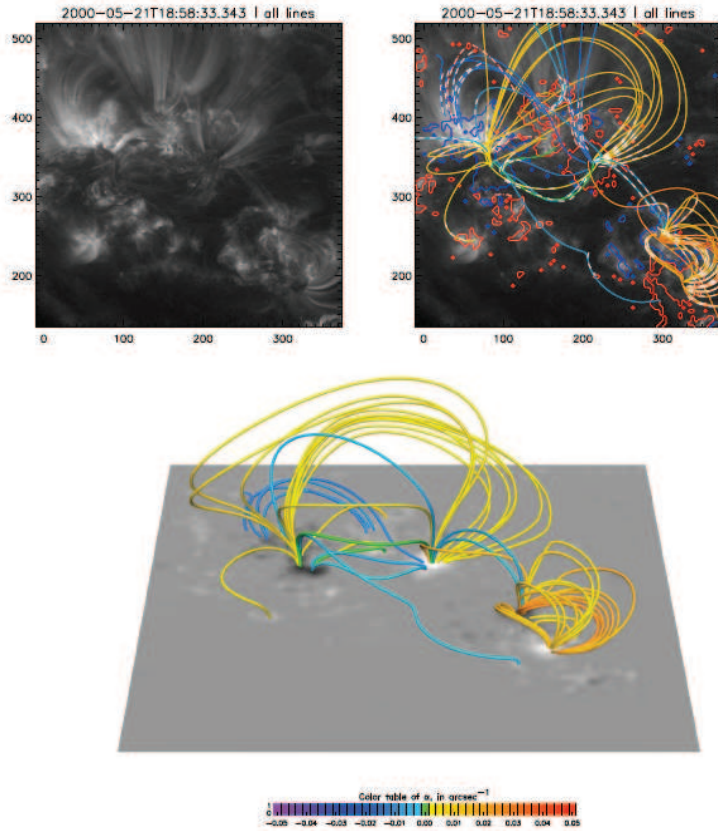


Figure 4. Reconstructed coronal field of AR9002 (North) and 9004 (South). Top left: the original TRACE 171 Å image. Top right: reconstructed field lines (solid) and smooth curves, traced visually over the visible coronal loops. For the successful fits (the success is estimated visually) the original loop is shown in dotted white and the field line in solid color. For the unsuccessful fits only the original loop is shown in dotted white-red. Different colors correspond to different values of  $\alpha$ . Bottom: 3D image of the reconstructed field lines, with field lines leaving the domain omitted.

loops manually traced to provide this information along all the apparent field lines. Figure 4 shows an example of the results from its application to AR pair 9002/9004 by Malanushenko et al. (2011).

Although the method uses constant- $\alpha$  extrapolations, it has been shown to yield accurate information about fully non-linear force-free fields (NLFFFs, Malanushenko et al., 2009). This information is, however, rather sparse: only known along observed coronal loops. Recently Malanushenko et al. (2012) have developed a method, called the Quasi-Grad-Rubin (QGR) technique, to use this sparse information to produce a volume-filling NLFFF. While similar information could be obtained from the photospheric magnetograms alone using traditional NLFFF extrapolation techniques (Schrijver et al., 2006; Metcalf et al., 2008; De Rosa et al., 2009), we prefer the QGR method because it makes use of the EUV

While the potential field provides an upper bound on the reconnection rate, the *actual* reconnection rate is measured using a combination of EUV imaging data and a coronal magnetic field model. First a model of the *actual* coronal field is built from EUV imaging data in combination with the photospheric magnetograms, using a method developed by the Co-I (Malanushenko) under previous SR&T funding (Malanushenko et al., 2009). Coronal loops are manually traced in an EUV image. A set of constant- $\alpha$  fields are extrapolated from a co-aligned magnetogram at a similar time. A single point on the loop image defines a line of points in each extrapolation volume (the line-of-sight). Field lines are initiated from each point and traced in both directions to the lower boundary. These curves are then projected back onto the plane-of-sky and compared *via* penalty function to the traced loop. The field line with the minimum penalty is deemed the best fitting<sup>1</sup> and used to estimate the magnetic twist parameter  $\alpha$  of that particular loop. It also provides the three-dimensional geometry of that loop and the field strength over its full length. The process is then repeated for all the

<sup>1</sup>There are several other criteria, all explained in Malanushenko et al. (2009).

data which is central to our analysis. In particular, the QGR will use the data from all the same interconnecting loops we use to derive the reconnection rate; there is no assurance that this same flux will interconnect in a NLFFF extrapolation. Our methodology is thus internally consistent between its magnetic field modeling and measurement of flux transfer.

### 2.2.2 The transferred flux

Provided we consider cases where new photospheric flux appears clearly distinct from the pre-existing AR, every magnetic field line connecting a new polarity to an old polarity is necessarily the result of magnetic reconnection. Here we measure how much interconnecting flux is being created by the reconnection. EUV images are formed into a co-aligned data cube. A strip of pixels is extracted from these, along a line clearly separating new from old ARs (see fig. 5). The strips from the entire data cube form a stack plot,  $I(x, t)$ , with one spatial dimension (along the strip) and time. The right panel of fig. 5 shows the  $171\text{\AA}$  stack plot used to identify loops connecting AR9754 to 9570. Each interconnecting loop appears as a streak in  $I(x, t)$  which can be identified automatically. Not all streaks, however, correspond to interconnecting loops. It is therefore necessary to verify that each streak is an interconnecting coronal loop and not some other bright feature or a loop which is not interconnecting. This step produces 43 verified interconnecting loops in the stack plot in fig. 5.

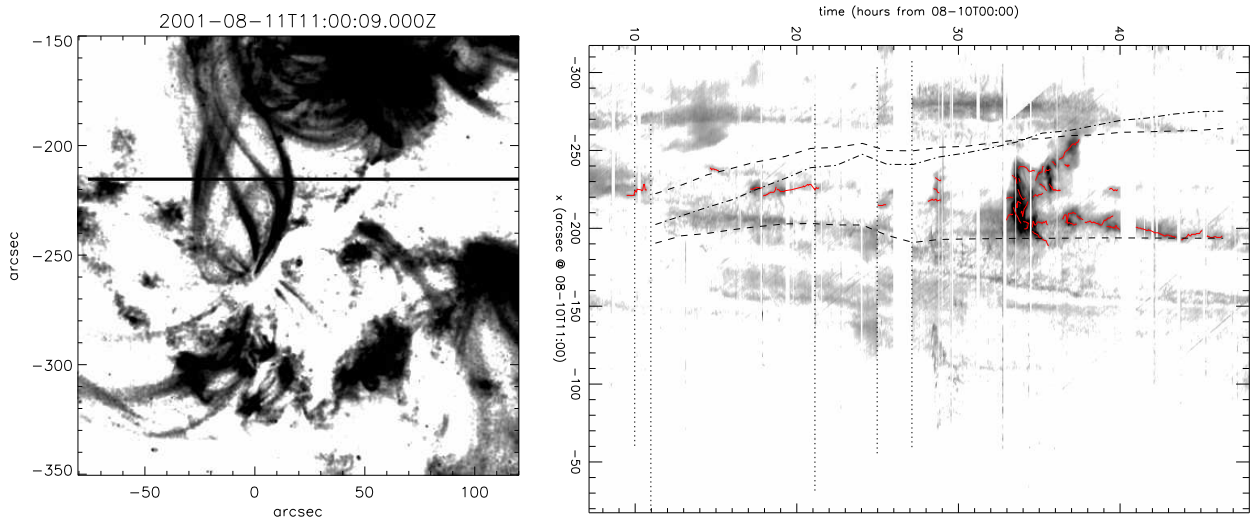


Figure 5. Loops interconnecting AR9570 (South) to AR9574 (North). Left panels shows a single TRACE  $171\text{\AA}$  image from Aug. 11, 11:00 ( $t = 35$ ). A horizontal strip is extracted to find loops interconnecting the ARs. Four such loops are evident. The right panel is a stack plot,  $I(x, t)$ , built up of all the extracted strips — time runs horizontally. Red curves show the streaks which have been identified as interconnecting loops.

Streak  $i$  in the stack plot reveals the position,  $(x_i, y_i)$ , diameter  $d_i$ , and time of first appearance,  $t_i$ , of interconnecting loop  $i$ . If loop  $i$  coincides with one of those fit by a magnetic model, then the field strength  $B_i$  at the slit position,  $(x_i, y_i)$ , may be found directly. Otherwise the value is interpolated from nearby loops which were fit, or it is evaluated from the volume-filling QGR field at a position estimated from the separatrix or nearby loops. The newly forged loop contains magnetic flux  $\delta\psi_i = \pi(d_i/2)^2 B_i$ , which must have been transferred across the separator by a reconnection electric field. Attributing this flux to time  $t_i$  produces an accumulated flux-transfer curve,  $\Phi_{21}(t)$ , such as the one shown in the bottom panel of fig. 3. The time derivative of this curve,  $\mathcal{E}_{21} = \dot{\Phi}_{21}$ , gives the *actual* EMF along the separator where magnetic reconnection is occurring, according to eq. (1).

In the case of ARs 9570/9754, significant flux transfer begins at about 8:00UT on 11-Aug, 24 hours after emergence began. The actual rate of flux transfer,  $\dot{\Phi}_{21} \simeq 10^{17}$  Mx/sec, is about six times the steady rate at which the potential field changes,  $\dot{\Phi}_{21}^{(v)} = 1.5 \times 10^{16}$  Mx/s. *It appears that coronal reconnection does not proceed at the rate it is driven.* Instead there is a delay (24 hours in this case) followed by rapid flux transfer over a brief (5 hour) interval. While the *mean* reconnection rate remains lower than that of the potential field (i.e. the driver) the *instantaneous* rate is far greater.

Since the interconnecting loops are forged by magnetic reconnection, their properties reveal details of the reconnection process. For example, distinct loops may result from a reconnection electric field which is transient and spatially patchy (Linton and Longcope, 2006; Longcope et al., 2009b). If this is the case then the distribution of loop diameters,  $\{d_i\}$ , relates to the distribution of electric field patch sizes within the current sheet. Similar reasoning has been applied to supra-arcade downflows (SADs) to infer the spectrum of electric field fluctuations in current sheets below CME flux ropes (McKenzie and Savage, 2011). The investigation described here yields this information for reconnection in the non-flaring corona.

### 2.3 Reconnection: Energy release

In addition to transferring magnetic flux into topologically distinct domains, reconnection facilitates the release of stored magnetic energy. Flux transfer is difficult to observe and must be measured using the innovative techniques described above. In contrast, there has been a significant effort devoted to using EUV and X-ray observations to measure energy release. We make use of these standard methods to compute the state of the plasma within the reconnected domain, and from that to compute the energy released by the reconnection.

The key to measuring plasma properties is two or more images made in spectral bands with different temperature responses. Two bands allow the calculation of a temperature and emission measure (EM) under an isothermal assumption. More bands allow more detailed characterization using differential emission measure (DEM). We have, in several previous investigations, used the complete range of AIA bands to produce DEMs and also used pairs of X-ray filters from *Hinode*/XRT to compute temperature and EM of post-reconnection flux systems. In all of these cases we found the XRT values agreed remarkably well with values obtained by integrating AIA-derived DEMs (Guidoni et al., 2015). We therefore expect that either method will produce comparable results for the integrated energetics of the post-reconnection plasma studied here.

The plasma properties, derived as described above, are used in a radiative loss function to compute the total power,  $P_{\text{rad}}$ , radiated, and total thermal energy content,  $U_{\text{th}}$ , of the coronal plasma in the interconnecting domain. The coronal field model is used to compute the lengths of the interconnecting coronal loops, from which we find the conductive cooling time,  $\tau_{\text{cond}}$ . The energy lost from the coronal plasma by conduction to the cooler chromosphere is  $P_{\text{cond}} = U_{\text{th}}/\tau_{\text{cond}}$  (Longcope et al., 2010). Adding to this the radiated loss,  $P_{\text{rad}}$ , yields the total loss,  $P$ , whose time integral is an energy loss which must have been first *added* to the plasma. Prior to the topological change of its field, this plasma was confined to loops of the old or new AR. Thus we do not expect its equilibrium heating needs to have been significantly changed by the reconnection. Based on that logic we assume that all or most of the added energy was released by the process of magnetic reconnection which created the new domain in the first place.

**Comparison of flux transfer rate,  $\dot{\Phi}$ , to energy loss rate,  $P$ , provides the essential characterization of reconnection at which the proposed investigation is aimed.** Figure 6 shows an example from a single AR (AR11112) into which additional flux has emerged (Tarr et al., 2014; Longcope and Tarr, 2015). Ratios of Ti-poly and Al-mesh filters of *Hinode*/XRT were used to

derive  $T$  and  $EM$  at 1-hour cadence. These quantities are used in a radiative loss function to compute the net radiated power,  $P_r$ , plotted in the right panel (black solid curve). A mean flux transfer rate,  $\dot{\Phi}_{21} \simeq 0.3 \times 10^{16}$  Mx/s was derived by mapping the footprint of the reconnected flux onto the radial field from an SDO/HMI vector magnetogram (lower left). The ratio of power to flux transfer rate rises to  $P_r/\dot{\Phi}_{21} \simeq 3 \times 10^{11}$  Amps over the 50 hours of flux emergence. Thus while flux transfer is fairly steady it is becoming increasingly effective at releasing energy. The explanation may lie in the fact that the actual flux transfer rate is below that required by a potential field (i.e.  $\dot{\Phi}_{21} < \dot{\Phi}_{21}^{(v)}$ ) and thus the flux difference,  $\Phi_{21}^{(v)} - \Phi_{21}$  (plotted in magenta), increases over time. This means the field must be growing increasingly non-potential, building up current, which results in greater energy release for the same flux transfer. This hypothesis was not, however, verified by Tarr et al. (2014), since they lacked a NLFFF of the kind we will produce using QGR.

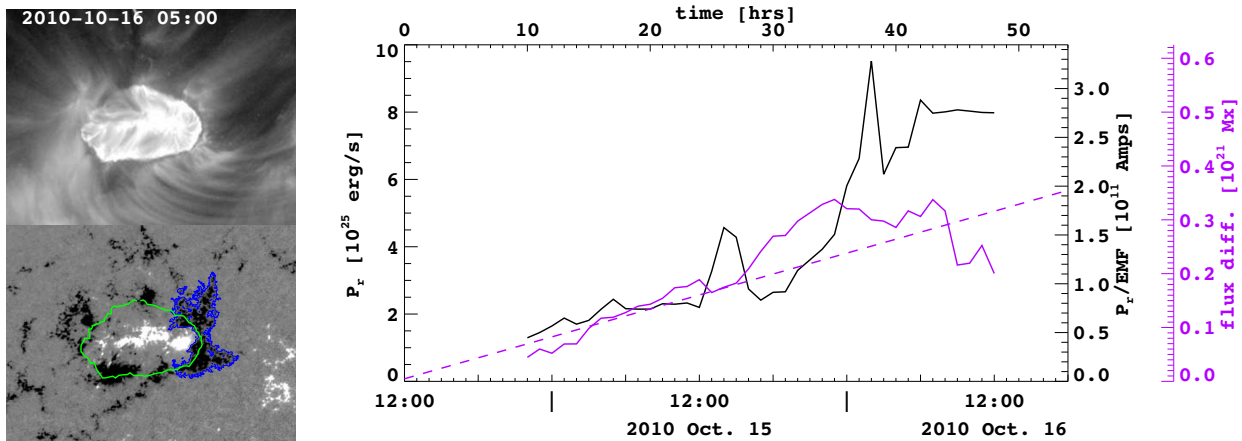


Figure 6. Flux transfer and radiative losses from AR1112 (Longcope and Tarr, 2015). The left column shows images from AIA 211Å of the flux overlying the emerging bipole (top) and the HMI magnetogram of the region. The green curve is the perimeter of the separatrix dome, which includes negative flux from the old polarity,  $N1$ , outlines in blue. The right panel shows the radiated power derived using a ratio of XRT images (black). The result of dividing this power by the observed EMF,  $\mathcal{E} = 3 \times 10^7$  Volts, can be read from the right axis. The difference  $\Phi_{21} - \Phi_{21}^{(v)}$  is plotted in magenta against the far right axis.

### 3 Proposed Work

The analysis described above has been applied once, with great success, to TRACE and SoHO/MDI data of ARs 9570/9574. Since then the method has been improved, but no comparable data set was found in the TRACE archive to apply the improved method. Now that SDO has accumulated an extensive bank of data from emerging active regions, we are ready to make full use of our method for quantitative measurements of magnetic reconnection. Its virtually continuous coverage, high time-cadence, unlimited field of view, and multiple band passes, make SDO/AIA far better suited to this task than was TRACE. We have no doubt that we will be able to obtain reconnection rates and energy release rates for between 8 and 16 new ARs.

We have identified 16 cases, during SDO operation (i.e. after 1 Sept. 2010), of AR emergence near central meridian, in close proximity to an existing AR, but far enough apart that the two are distinct; these are listed in Table 1. Figure 7 shows two cases (#1 and #3), both offering clear potential for our reconnection study. 171Å images from AIA (right column) clearly show many interconnecting loops. In each case there is ample separation between ARs to draw a line (white) across which all interconnecting loops must pass. We will extract a strip along that line, exactly as in fig. 5, to produce a stack plot

and identify all interconnecting flux.

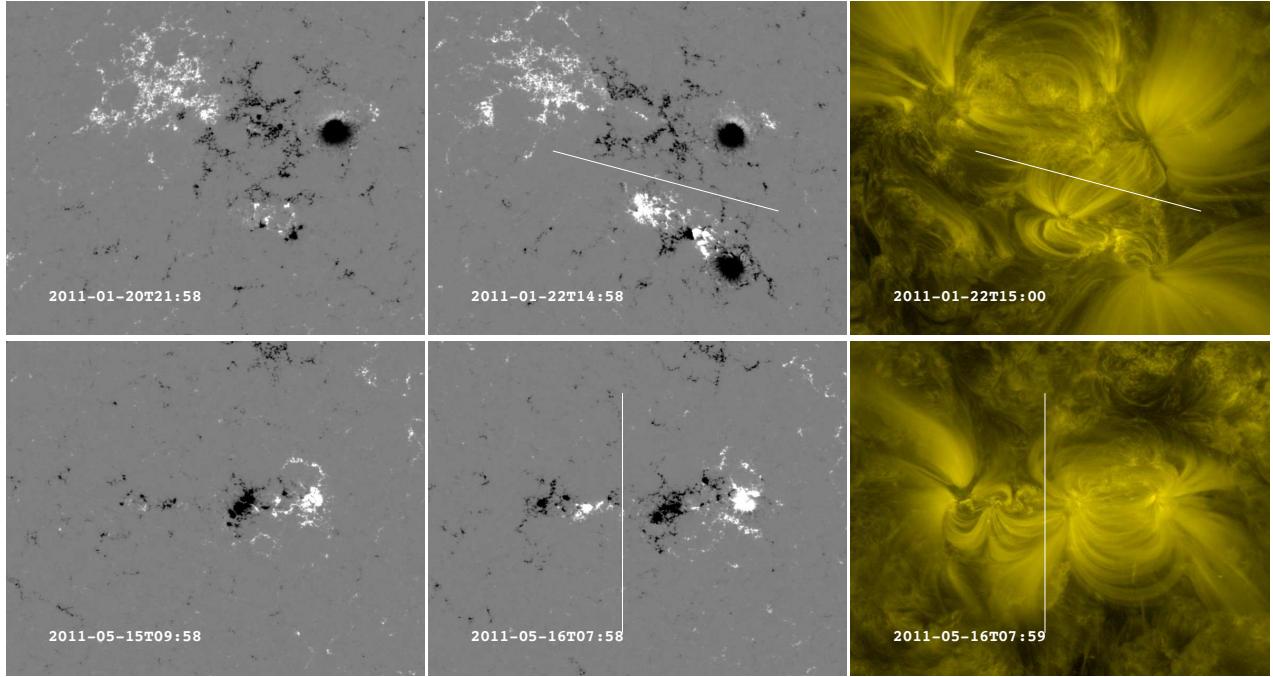


Figure 7. Two of the 16 cases proposed for study. Left and center columns are HMI line-of-sight magnetograms (grey-scale saturated at  $\pm 500$  G) from before (left) and after (center) emergence. The right column shows a  $171\text{\AA}$  AIA image from the same time as the second magnetogram (logarithmic scaling). A white line shows a possible strip from which a complete set of interconnecting loops may be identified. In the top row AR1149 emerges at N17W04, to the south of AR1147. In the bottom row AR1217 emerges at S18E36, to the east of AR1214.

### 3.1 Case selection

The full list of AR emergences, Table 1, spans the entirety of the SDO archive to date, and fairly represents both hemispheres. Several of the regions had no flares, C-class or above, attributed to them and will provide a sample of energization through quiescent reconnection. Among the remainder, several had a handful of small flares, while others had a dozen or more, including M-class flares and one (#14) had an X1 flare. Some pairs, such as #1 shown along the top row of fig. 7, consist of bipoles of comparable size. Others are mis-matched in size; in #3 (bottom row of fig. 7) the new region is the smaller one, but in case #6 (not shown) it is by far the larger one.

#	date y-m-d	ARs old/new	helio. loc.	ang. sep.	flares C/M	#	date y-m-d	ARs old/new	helio. loc.	ang. sep.	flares C/M/X
1	2011-01-20	1147/1149	N17W04	$6.3^\circ$	11/1	9	2012-01-14	1395/1398	N18E04	$8.2^\circ$	3/0
2	2011-02-17	1161/1162	N17W05	$7.2^\circ$	20/4	10	2012-04-18	1458/1460	N18E17	$9.0^\circ$	5/0
3	2011-05-15	1214/1217	S18E36	$5.1^\circ$	0/0	11	2013-01-10	1649/1655	S22W02	$5.1^\circ$	0/0
4	2011-08-29	1277/1282	N23E01	$6.1^\circ$	0/0	12	2013-02-19	1671/1678	N09W26	$9.8^\circ$	10/0
5	2011-10-12	1313/1320	S19W22	$8.1^\circ$	7/0	13	2013-10-13	1865/1870	S13W05	$9.2^\circ$	18/3
6	2011-10-29	1334/1335	N15E40	$8.6^\circ$	7/0	14	2013-11-11	1893/1900	S15E15	$9.2^\circ$	31/4/1
7	2011-12-05	1367/1370	S29E25	$8.0^\circ$	18/0	15	2013-12-03	1908/1914	S18W19	$7.6^\circ$	0/0
8	2011-12-18	1381/1382	S18E36	$6.0^\circ$	11/0	16	2014-04-14	2036/2037	S10E29	$9.4^\circ$	31/1

Table 1. A list of existing/emerging region pair for analysis.

Our list was compiled from AR emergence data and appears to include at least one case (#14) in which a cursory inspection reveals few interconnecting loops — possibly none. We intend to perform the

same search for interconnecting loops for this as for the other cases. If we ultimately conclude that no reconnection occurs between the ARs, then we must search for an explanation. We are almost certain that the potential field will have  $\Phi_{21}^{(v)} > 0$ , so some current layer must separate the unreconnected ARs. The question we would need to answer is why the current persists in this case, and not in others. One possibility is that hypothesized reconnection-threshold condition is never met. This case will provide us with a measurement bounding this threshold condition.

We hope to analyze all 16 cases on the list, but cannot rule out unforeseen difficulties. For example adverse geometry in a few cases might make unambiguous identification of interconnecting loops difficult. Or, the analysis may require time at the upper end of our estimates (see below). In the worst case we will certainly be able to analyze half the cases in Table 1, yielding results from eight (8) new reconnection episodes to add to the one presently in the literature (ARs 9570/9574 in Longcope et al., 2005).

### 3.2 Flux transfer measurement

The reconnected flux will be computed by extracting a strip of pixels from a cube of co-aligned AIA images. Interconnecting loops typically live 20 minutes or more (Longcope et al., 2005) so the full 12-second cadence is not necessary for this study. We plan to use sub-field images at 1-minute cadence. It has been generally recognized that 171Å images show loops with the greatest clarity and contrast (see e.g. fig. 7). This band-pass was used in Longcope et al. (2005) and we will use it for this study.

There is a possibility that, following its energization by reconnection, some plasma does not cool to temperatures low enough to appear in 171Å (cooler than  $\sim 10^6$  K). In this case some portion of reconnected flux will be missed by the 171Å analysis. This possibility was raised by Longcope et al. (2005), but could not be verified or corrected with the TRACE data available. Here we will assess the possible undercounting by repeating the analysis for cubes of 211Å images ( $\sim 2 \times 10^6$  K) and then 335Å images ( $\sim 3 \times 10^6$  K). We expect the 211Å images to show loops with almost the same clarity as those from 171Å. We will try to match the loops identified by these two steps in order to compute the actual cooling times for a subset of loops. Loops are generally less clearly defined in 335Å images either due to its broader temperature response, or longer time spent within the temperature band by more slowly cooling plasma. In any event, we expect to find fewer clearly defined streaks in the 335Å stack plot. Finally, for a few cases we will perform the analysis using 94Å images ( $\sim 6 \times 10^6$  K), to assess the prevalence of very hot plasma. We expect this kind of plasma temperature when reconnection is especially rapid, for example in a flare. We will also search for it in less rapid reconnection.

Programs written for Longcope et al. (2005) and improved under subsequent SR&T funding can be quickly adapted for SDO/AIA data. From the co-aligned data cube, they extract a strip of arbitrary orientation, create a stack plot,  $I(x, t)$ , and automatically identify streaks in it. An image is then presented for each streak so that the user may confirm its correspondence to a genuine interconnecting loop. The user manually confirms the genuine identifications and rejects cases of non-loop brightenings or loops which do not clearly connect new to old flux. Each interconnecting loop is then characterized by its plane-of-sky position  $(x_i, y_i)$ , time of appearance  $t_i$ , lifetime  $\tau_i$ , and diameter  $d_i$ . Given the advanced stage of the existing software we expect to spend minimal time adapting it to AIA data, and about 3 days to run each emergence.

### 3.3 The magnetic model

The first step in the magnetic modeling is for a user (our graduate student) to trace out all the loops in an EUV image. This will be done for a sub-set of the same 171Å data cube used above, down-sampled to a 20-minute cadence. For most images only interconnecting loops will be traced. This

step is independent of the stack-plot-streak location, however, since the two involve common data, we expect most or all of the verified streaks to match loops traced in this step.

Following the methodology of Malanushenko et al. (2009), the interconnecting loops traced by hand will be fit to field lines integrated from constant- $\alpha$  fields. These fields will be extrapolated from SDO/HMI data from a time within 2 hours. The constant- $\alpha$  extrapolations can use either radial field from ambiguity-resolved vector magnetograms or line-of-sight data. In either case the magnetogram is coarsened, mapped to a vertical projection and then used as the lower boundary for a set of fields with  $\alpha$  taking on  $N_\alpha$  distinct values, positive, negative, and zero (Malanushenko et al., 2009). For each traced loop, a series of field lines is integrated from each of the  $N_\alpha$  fields, and all are projected onto the plane-of-sky and compared by penalty function to the actual loop. The field line minimizing the penalty function (i.e. the best fit) is then taken to provide the configuration and  $\alpha$  value of that loop. The height and field strength,  $B_i$ , at the point it crosses the strip will be associated with the streak identified in the flux transfer calculation. The result will be a value of flux  $\delta\psi_i = \pi(d_i/2)^2 B_i$  for the streak from which the reconnection flux curve  $\Phi_{21}(t)$ , like that in fig. 3, is computed.

The proposing team has developed this field-modeling technique and applied it several times to AIA data in same way we will in this project. In our experience, each 171Å image will have between 3 and 50 loops, and will take on average 10–20 minutes to completely trace them all. The 144 images from a 48-hour data cube will therefore take about one week of student-dedicated time.

While the student is tracing the loops, an automated script will be generating and storing constant- $\alpha$  extrapolation cubes at a rate of, typically, one set of  $N_\alpha$  cubes every 6–12 hours, depending on the degree of coarsening used (we find coarsening to one-quarter HMI’s original resolution produces coronal field lines of sufficient accuracy for our purpose) and the value of  $N_\alpha$  (we have found 21–41 to be sufficient). We schedule two weeks to produce a full set of  $N_\alpha$  fields for each of the 24 magnetograms spanning the 48-hour emergence.

Once the loops are traced, and early field sets are completed, the student will begin the process of supervising the loop fitting. This is not a trivial process (Malanushenko et al., 2009) and will require about one more week of student-dedicated time. All told we expect a complete 48-hour emergence to be modeled after 2.5 weeks of dedicated effort. Cases of more extended emergence will take proportionately longer.

Performing the Quasi-Grad-Rubin (QGR) extrapolation requires significantly more time than the simple constant- $\alpha$  step. We will perform this modeling for only 6–8 times during the emergence. For each of these times loops must be traced throughout the active region complex — not just interconnecting loops. These are fit in the same manner as the interconnecting loops. The complete set of loops is then used in the QGR algorithm (Malanushenko et al., 2012) to obtain a full NLFFF, typically after a full week of computer time per field.

These QGR fields, available only at a cadence of 6–8 hours, will provide important supplementary information concerning the corona. First, they contain current and therefore free magnetic energy which are both expected to be related to magnetic reconnection. We will make direct comparisons of the flux transfer rate and energy release rate to the free energy and current in the coronal field. Second, the QGR field includes a full volume of reconnected flux, as opposed to isolated visible coronal loops. Integrating the flux within the volume provides an alternative measurement of reconnection flux,  $\Phi_{21}^{(\text{QGR})}(t)$ , albeit at lower time cadence. Comparison between these two will provide unique information concerning the effectiveness with which energy deposited into coronal plasma results in a visible loop. Finally, the surface overlying the interconnecting volume is a separatrix, and contains a separator. We therefore have, in the NLFFF model, a location to which we can attribute the reconnection EMF. It is

the curve along which the electric field is integrated in eq. (1).

### 3.4 Energetics

The final element in our analysis will be measuring the energy release due to magnetic reconnection. The set of interconnecting loops traced for the magnetic model will be used to define the time-evolving region containing reconnected flux. A simple, closed region, defined by the convex hull of the loop images, will be used for this. This region will be mapped onto a set of multi-wavelength images to obtain a map of temperature and emission measure (EM) covering the reconnected flux. The map can be found from filter ratios of *Hinode*/XRT image pairs (Narukage et al., 2011) when the data are available. Our preliminary search of the XRT archive indicates that data are available for approximately half of our AR pairs. Otherwise, the excellent temperature coverage and diagnostic power of AIA’s multiple EUV passbands provide a means to resolve, spatially and temporally, the plasma EM as a function of temperature. A set of six co-aligned AIA images (171, 193, 211, 335, 94 and 131 Å) are used to find a DEM in each pixel. In cases where *Hinode*/XRT also observed the loops, the AIA data are supplemented with XRT data to further constrain the highest-temperature bins in the DEM. The team has experience using the `xrt_dem_iterative2` routine and the DEM solver developed by Plowman et al. (2013), both of which use the AIA and XRT response curves published in SolarSoft. In our testing, as part of a project funded by a previous LWS grant, we have determined that although `xrt_dem_iterative2` is far slower than the Plowman et al. (2013) algorithm and the procedure due to Hannah and Kontar (2012), it has the advantage of enforcing positive definiteness in the returned densities and emission measures whereas the faster algorithms are not positive-definite.

The DEM computed as described can be used to compute a total EM and mean temperature in each pixel. We have found that this process closely matches the results from the XRT filter ratio (Guidoni et al., 2015). Moreover, the integrated energetics, radiative and conductive losses, are well modeled by even the cruder filter ratio method. For cases of steady reconnection, such as that shown in fig. 3, we will produce integrated quantities at about 1-hour cadence to produce a power curve,  $P(t)$ , similar to that in fig. 6. In some cases the reconnection occurs partly through flares, whose energetics must be resolved at higher cadence. Since we are only following the thermal evolution, the gradual phase must be resolved, which can be achieved by cadences no faster than 15 minutes.

## 4 Expected Results & Perceived Impact

The analysis proposed here will provide, at different stages, answers to each of the five questions posed in Sec. 1. The most significant result of applying the analysis pipeline outlined above to an emergence case from Table 1 will be a measurement of both the rate of topological change,  $\dot{\Phi}_{21}$ , and the rate of energy release,  $P(t)$ , accompanying the emergence. The relation between these two is the essential product of any and every theory of magnetic reconnection. In spite of this centrality, the relationship has rarely been compared to observation. This comparison is the primary objective of the investigation proposed here.

The curves alone will provide immediate answers to several questions about reconnection. Does reconnection proceed at the same rate the flux is being driven? (Q1) The first application by Longcope et al. (2005) suggests the answer is “No”. That case showed a clear delay of  $\sim 24$  hours between the initiation of emergence and the onset of significant reconnection. We cannot say whether this scenario is common, rare, or unique. At least one previous study by Schrijver et al. (2005) found evidence for a delay of similar scale ( $\sim 24$  hours) before newly emerged ARs relaxed from their non-potential state. Moreover, a reconnection-delay is necessary if the coronal field is to store magnetic energy, whose release is credited with supplying coronal heat (Longcope, 1996). Each case we analyze will add one

more data point to our knowledge of the delay preceding reconnection.

Having observed the reconnection curves,  $\Phi_{21}(t)$ , for several cases, we can begin to seek an explanation for its behavior. The magnetic modeling will reveal the helicity of each AR as well as the total free energy. Figure 4 shows a case (9002/9004) where the ARs have the same sense of twist ( $\alpha > 0$  in both) and the interconnecting flux has the opposite ( $\alpha < 0$ ). Does the relative sense of helicity affect the rate of reconnection or the pre-reconnection delay? (Q2) Once we have several observations we should be in a position to answer this important question. Some previous investigations have suggested a link of this nature (Ono et al., 1993; Canfield et al., 1996), to which our study will provide additional details. Finally, we can test the hypothesis that a threshold in helicity, net current, or free magnetic energy may be the trigger for the onset of reconnection (Malanushenko et al., 2009). All of these properties will be measured in our volume-filling QGR field. Although recent numerical models have tried to determine the conditions responsible for a threshold (e.g. Cassak et al., 2006; Galsgaard et al., 2007), there appears to be little agreement yet: Galsgaard et al. (2007) predicts a delay of about 20 *minutes*. Establishing by observational means the range of delays between emergence and reconnection is a crucial first step towards constraining these models and understanding the origin of a threshold.

The combination of reconnection rate,  $\dot{\Phi}_{21}(t)$ , and power,  $P(t)$ , will provide the most novel contribution of the proposed study. (Q3) The topological change which constitutes magnetic reconnection does not automatically lead to heating or energy release. Theoretical models from the very first (Sweet, 1958; Parker, 1957; Petschek, 1964) have attempted to link the two. To date there have been very few direct measurement of both by which the proposed link could be tested. To wit, if the energy deposition measured in  $P(t)$  is attributable entirely to magnetic reconnection then the two would necessarily vary together. In theoretical models of magnetic reconnection they will be proportional with a constant related to the net current in the sheet across which the reconnection occurs. This correlation should be evident in each example of the two curves measured in our investigation. The accumulation of many cases will permit the correlation to be tested statistically.

Earlier attempts to make such a measurement have not yielded clear results. The prototypical study by Longcope et al. (2005) had multi-bandpass data from *Yohkoh/SXT*, but only during two isolated intervals during the 41-hour emergence. In the study by Tarr et al. (2014), whose data was used in fig. 6, emergence occurred *within* an existing AR, making  $\dot{\Phi}_{21}(t)$  more difficult to measure. Furthermore, the reconnected loops were never clearly identified, so conductive losses could not be computed. The study proposed here will yield the first cases where both quantities can be clearly measured and easily compared. Better yet, it will make these measurements in 8–16 different episodes.

Finally, the investigation will characterize the details of magnetic reconnection at the same time it quantifies its global nature. According to eq. (1), the flux transfer rate,  $\dot{\Phi}_{21}$ , corresponds to an EMF along the topological boundary overlying the interconnecting flux: the *separator*. (Q4) Applying this reasoning to flares (Forbes and Priest, 1984; Fletcher and Hudson, 2001; Qiu et al., 2002) or to quiescent reconnection episodes (Longcope et al., 2005; Tarr et al., 2014), using a single separator, like that in a potential field, has yielded electric field values far above the Dreicer value. This is generally dismissed as impossible. One likely resolution is that the observed topological change is occurring at a large number of parallel separators, known to occur in non-potential field (Parnell et al., 2008, 2010). This kind of “patchy” reconnection can proceed far more rapidly than the single-separator (i.e. single X-line) variety (Loureiro et al., 2007; Bhattacharjee et al., 2009). It will also produce a set of distinct reconnected flux tubes instead of a single monolithic volume (Linton and Longcope, 2006).

One of the first products from this data set will be the distribution function characterizing reconnected flux tubes,  $\{d_i\}$ . (Q5) A study of supra-arcade downflows, (SADs) by (McKenzie and Savage,

2011) found their areas had a log-normal distribution. At the time these features were believed to be flux tubes formed by reconnection in a current sheet left in the wake of a CME. This observation has been explained by several theoretical models of magnetic reconnection (Guo et al., 2013; Cassak et al., 2013; Lynch et al., 2014). Recent studies have cast doubt on that interpretation (Savage et al., 2012), leaving the significance of the area distributions uncertain. There is no doubt, however, that the coronal loops observed in the study proposed here will correspond to reconnected flux. Their distribution can therefore be interpreted using the theoretical models originally applied to SADs.

### Sources of uncertainty

Our measurement of reconnected flux and energy release will be subject to several uncertainties for which we will account as much as possible. Statistical uncertainty will be accounted for using standard error analysis. Individual measurements are accumulated into global quantities, whose error bars will thus be relatively small. The most significant uncertainties will therefore arise from *systematic* errors.

The greatest systematic contribution to the flux measurement stems from our assumption that *all* magnetic flux which is topologically changed will appear in loop form in EUV imaging data. The assumption is equivalent to assuming first that reconnection releases energy, and second that excess energy deposited into a loop will render it denser, and therefore visible against the background corona. The first assumption is the main focus of our investigation, and if we find it to be false then we will overturn a fundamental tenet of reconnection modeling. If the second assumption is false, and heating is ineffective at producing a visible corona, perhaps only occasionally, this will reveal itself through a systematic discrepancy between the flux measured by EUV (at high cadence) and that measured from the QGR field (at a lower cadence). Finally, if reconnected flux visibility is limited by plasma temperature, the discrepancy will appear in the comparison of 171Å and 211Å loop data.

The main source of systemic errors in the energetics would arise from losses for which we have not accounted. The interconnecting flux system consists, by definition, of closed field lines so no energy will be lost to flows to the solar wind. We do not account explicitly for non-thermal particles, but expect any contribution they may make, at least most of the time, to be captured by our measurement. Even excluding the few significant flares in our sample, non-thermal particles may be responsible for carrying energy and depositing it in the thick target of the chromosphere (Hannah et al., 2008; Testa et al., 2014). Virtually all of that energy will be manifest as heat, which is captured in our analysis provided it results in emission detectable in one of the AIA passbands. Finally, energy released by reconnection and carried out of the interconnecting domain by fast magnetosonic waves (Longcope and Tarr, 2012), will need to be accounted for by a crude multiplicative loss factor.

## 5 Relevance to NASA’s Programs

The proposed investigation addresses a Goal identified in the NRC Decadal Survey (Decadal Survey, 2013), namely to “Discover and characterize fundamental processes that occur both within the heliosphere and throughout the universe”, which includes as a specific examples magnetic reconnection. Additionally, magnetic reconnection is identified in NASA’s Heliophysics Roadmap (Heliophysics Roadmap, 2009) as a Research Focus Area relevant to the Objective of “Understand[ing]the Sun and its Effects on Earth and the Solar System”. Through the combination of observational measurements and modeling, this investigation is relevant to two Priority Investigations in the reconnection Research Focus Area of the Roadmap: “What are the fundamental physical processes and topologies of magnetic reconnection?”, and “How are plasmas and charged particles heated and accelerated?”

## 6 Plan of Work

This investigation will be conducted primarily by an MSU Physics PhD student assisted by a team of senior personnel. The student has not yet been identified, but there are several candidates among the second-year graduate students currently completing their course-work at MSU. The proposed project includes some labor-intensive steps, such as tracing loops, which will provide an opportunity for a beginning graduate student researcher to learn about Solar Physics data. The student will become familiar enough with the process that he or she will be able to streamline it by writing scripts and driver programs. At that point it will be possible for the student to supervise an undergraduate researcher in the most straight-forward tasks. Indeed, the Co-I (Malanushenko) did this while she was an MSU graduate student, supervising a Junior from Berea College (Kentucky) participating in MSU's 10-week Solar Physics Research Experiences for Undergraduates (REU) program (Malanushenko et al., 2011). We expect that the investigations proposed here will provide summer projects for two REU students over the summers of 2016 and 2017.<sup>2</sup>

The graduate student will work closely with all three senior members of the proposing team. Prof. McKenzie will work primarily on the energetics computations. This will involve processing and co-aligning *Hinode*/XRT data, when available, and SDO/AIA data in other cases. Prof. McKenzie is a Co-I on both instruments, and intimately familiar with their data. He will work with the student to produce estimates of the energy loss,  $P(t)$ , from the region of interconnecting loops. He will also serve on the student's thesis committee.

Dr. Malanushenko will assist with the extracting of stack plots and with the development of magnetic models. She led the effort to improve the stack-plot method, and was responsible for the development of both the loop-fitting method and the QGR extrapolation. She is currently an ASP fellow at HAO, but will take leave from the fellowship for intervals during each year (1 month during Y1 and 3 months during Y2). During her leave she will be appointed as a research scientist at MSU, but will probably continue to work from Boulder, CO.<sup>3</sup> During Y1 she will supervise and train the student in stack-plot extraction, loop tracing, and fitting. Following this the student should be able to analyze at least 6 ARs to that level in Y1. Beginning Y2 she will assist the student with the more time-consuming, and technically challenging QGR method. This enters only the final, interpretive portion of the investigation, so it is natural to delay it until later.

The PI will supervise the project as a whole and will assist the student in the photospheric analysis, and in the final interpretation of the reconnection measurements. He will also probably serve as the chair of the student's thesis committee. The majority of his effort will be covered by his state salary for education and graduate research supervision.

## 7 Data Sharing Plan

The data materials to be produced in the course of this project consist of scientific findings from data analysis, which will be disseminated to the community via conference presentations and refereed publications.

---

<sup>2</sup>The REU program is funded by NSF, so no expenses related to the REU students are borne by this grant. The usual stipend will be paid to the MSU graduate student, supervising the REU student.

<sup>3</sup>She previously held an MSU appointment until Oct. 2014, even as she worked from Palo Alto at Lockheed-Martin.

## References

- Barnes, G., Longcope, D. W., and Leka, K. D. 2005, “Implementing a Magnetic Charge Topology Model for Solar Active Regions”, *ApJ* **629**, 561.
- Bhattacharjee, A., Huang, Y.-M., Yang, H., and Rogers, B. 2009, “Fast reconnection in high-Lundquist-number plasmas due to the plasmoid instability”, *Phys. Plasmas* **16**, 112102.
- Canfield, R. C., Pevtsov, A. A., and McClymont, A. N. 1996, “Magnetic chirality and coronal reconnection”, in Bentley, R. D. and Mariska, J. T., editors, *Magnetic reconnection in the solar atmosphere*, pp. 341–346, ASP.
- Cassak, P. A., Drake, J. F., Gosling, J. T., Phan, T.-D., Shay, M. A., and Shepherd, L. S. 2013, “On the Cause of Supra-arcade Downflows in Solar Flares”, *ApJ. Lett.* **775**, L14.
- Cassak, P. A., Drake, J. F., and Shay, M. A. 2006, “A Model for Spontaneous Onset of Fast Magnetic Reconnection”, *ApJ* **644**, L145.
- De Rosa, M. L., Schrijver, C. J., Barnes, G., Leka, K. D., Lites, B. W., Aschwanden, M. J., Amari, T., Canou, A., McTiernan, J. M., Régnier, S., Thalmann, J. K., Valori, G., Wheatland, M. S., Wiegmann, T., Cheung, M. C. M., Conlon, P. A., Fuhrmann, M., Inhester, B., and Tadesse, T. 2009, “A Critical Assessment of Nonlinear Force-Free Field Modeling of the Solar Corona for Active Region 10953”, *ApJ* **696**, 1780.
- Committee on a Decadal Strategy for Solar and Space Physics (Heliophysics), 2013, *Solar and Space Physics: A Science for a Technological Society*, National Academies Press, Washington, DC.
- Fletcher, L. and Hudson, H. 2001, “The Magnetic Structure and Generation of EUV Flare Ribbons”, *Sol. Phys.* **204**, 69.
- Forbes, T. G. and Priest, E. R. 1984, “Reconnection in Solar Flares”, in Butler, D. and Papadopoulos, K., editors, *Solar Terrestrial Physics: Present and Future*, pp. 35–39, NASA.
- Galsgaard, K., Archontis, V., Moreno-Insertis, F., and Hood, A. W. 2007, “The Effect of the Relative Orientation between the Coronal Field and New Emerging Flux. I. Global Properties”, *ApJ* **666**, 516.
- Guidoni, S. E., McKenzie, D. E., Longcope, D. W., Plowman, J. E., and Yoshimura, K. 2015, “Temperature and Electron Density Diagnostics of a Candle-Flame Shaped Flare”, *ApJ*, submitted.
- Guo, J., Emslie, A. G., and Piana, M. 2013, “The Specific Acceleration Rate in Loop-structured Solar Flares - Implications for Electron Acceleration Models”, *ApJ* **766**, 28.
- Hannah, I. G., Christe, S., Krucker, S., Hurford, G. J., Hudson, H. S., and Lin, R. P. 2008, “RHESSI Microflare Statistics. II. X-Ray Imaging, Spectroscopy, and Energy Distributions”, *ApJ* **677**, 704.
- Hannah, I. G. and Kontar, E. P. 2012, “Differential emission measures from the regularized inversion of Hinode and SDO data”, *A&A* **539**, A146.
- Heliophysics Roadmap Team, 2009, *Heliophysics: The Solar and Space Physics of a New Era*, NASA, Washington, DC.
- Linton, M. G. and Longcope, D. W. 2006, “A model for patchy reconnection in three dimensions”, *ApJ* **642**, 1177.
- Longcope, D. and Tarr, L. 2012, “The Role of fast magnetosonic waves in the release and conversion via reconnection of energy stored by a current sheet”, *ApJ* **756**, 192.
- Longcope, D. W. 1996, “Topology and current ribbons: A model for current, reconnection and flaring in a complex, evolving corona”, *Sol. Phys.* **169**, 91.
- Longcope, D. W., Barnes, G., and Beveridge, C. 2009a, “Effects of partitioning and extrapolation on the connectivity of potential magnetic fields”, *ApJ* **693**, 97.
- Longcope, D. W., Des Jardins, A. C., Carranza-Fulmer, T., and Qiu, J. 2010, “A Quantitative Model of Energy Release and Heating by Time-dependent, Localized Reconnection in a Flare with a Thermal Looptop X-ray Source”, *Sol. Phys.* **267**, 107.
- Longcope, D. W., Guidoni, S. E., and Linton, M. G. 2009b, “Gas-dynamic shock heating of post-flare loops due to retraction following localized, impulsive reconnection”, *ApJ. Lett.* **690**, L18.
- Longcope, D. W., McKenzie, D., Cirtain, J., and Scott, J. 2005, “Observations of separator reconnection to an emerging active region”, *ApJ* **630**, 596.
- Longcope, D. W. and Tarr, L. A. 2015, “Relating magnetic reconnection to coronal heating”, *Proc. Roy. Soc. A*, in press.

- Loureiro, N. F., Schekochihin, A. A., and Cowley, S. C. 2007, “Instability of current sheets and formation of plasmoid chains”, *Phys. Plasmas* **14**, 100703.
- Lynch, B. J., Edmondson, J. K., Kazachenko, M. D., and Guidoni, S. E. 2014, “Reconnection Properties of Large-Scale Current Sheets During Coronal Mass Ejection Eruptions”, *ArXiv e-prints*, 1410.1089.
- Malanushenko, A., Longcope, D. W., Fan, Y., and Gibson, S. E. 2009, “Additive Self-helicity as a Kink Mode Threshold”, *ApJ* **702**, 580.
- Malanushenko, A., Longcope, D. W., and McKenzie, D. E. 2009, “Reconstructing the Local Twist of Coronal Magnetic Fields and the Three-Dimensional Shape of the Field Lines from Coronal Loops in EUV and X-Ray Images”, *ApJ* **707**, 1044.
- Malanushenko, A., Schrijver, C. J., DeRosa, M. L., and Wheatland, M. S. 2014, “Using Coronal Loops to Reconstruct the Magnetic Field of an Active Region before and after a Major Flare”, *ApJ* **783**, 102.
- Malanushenko, A., Schrijver, C. J., DeRosa, M. L., Wheatland, M. S., and Gilchrist, S. A. 2012, “Guiding Non-linear Force-free Modeling Using Coronal Observations: First Results Using a Quasi-Grad-Rubin Scheme”, *ApJ* **756**, 153.
- Malanushenko, A., Yusuf, M. H., and Longcope, D. W. 2011, “Direct Measurements of Magnetic Twist in the Solar Corona”, *ApJ* **736**, 97.
- McKenzie, D. E. and Savage, S. L. 2011, “Distribution Functions of Sizes and Fluxes Determined from Supra-arcade Downflows”, *ApJ* **735**, L6.
- Metcalf, T. R., De Rosa, M. L., Schrijver, C. J., Barnes, G., van Ballegoijen, A. A., Wiegmann, T., Wheatland, M. S., Valori, G., and McTiernan, J. M. 2008, “Nonlinear Force-Free Modeling of Coronal Magnetic Fields. II. Modeling a Filament Arcade and Simulated Chromospheric and Photospheric Vector Fields”, *Sol. Phys.* **247**, 269.
- Narukage, N., Sakao, T., Kano, R., Hara, H., Shimojo, M., Bando, T., Urayama, F., Deluca, E., Golub, L., Weber, M., Grigis, P., Cirtain, J., and Tsuneta, S. 2011, “Coronal-Temperature-Diagnostic Capability of the Hinode X-Ray Telescope Based on Self-Consistent Calibration”, *Sol. Phys.* **269**, 169.
- Ono, Y., Morita, A., Katsurai, M., and Yamada, M. 1993, “Experimental investigation of three-dimensional magnetic reconnection by use of two colliding spheromaks”, *Phys. Fluids B* **5**, 3691.
- Parker, E. N. 1957, “Sweet’s mechanism for merging magnetic fields in conducting fluids”, *J. Geophys. Res.* **62**, 509.
- Parnell, C. E., Haynes, A. L., and Galsgaard, K. 2008, “Recursive Reconnection and Magnetic Skeletons”, *ApJ* **675**, 1656.
- Parnell, C. E., Maclean, R. C., and Haynes, A. L. 2010, “The Detection of Numerous Magnetic Separators in a Three-Dimensional Magnetohydrodynamic Model of Solar Emerging Flux”, *ApJ* **725**, L214.
- Petschek, H. E. 1964, “Magnetic field annihilation”, in Hess, W. N., editor, *AAS-NASA Symposium on the Physics of Solar Flares*, pp. 425–439, Washington, DC, NASA.
- Plowman, J., Kankelborg, C., and Martens, P. 2013, “Fast Differential Emission Measure Inversion of Solar Coronal Data”, *ApJ* **771**, 2.
- Qiu, J., Lee, J., Gary, D. E., and Wang, H. 2002, “Motion of Flare Footpoint Emission and Inferred Electric Field in Reconnecting Current Sheets”, *ApJ* **565**, 1335.
- Savage, S. L., McKenzie, D. E., and Reeves, K. K. 2012, “Re-interpretation of Supra-arcade Downflows in Solar Flares”, *ApJ. Lett.* **747**, L40.
- Schrijver, C. J., DeRosa, M. L., Metcalf, T. R., Liu, Y., McTiernan, J., Régnier, S., Valori, G., Wheatland, M. S., and Wiegmann, T. 2006, “Nonlinear Force-Free Modeling of Coronal Magnetic Fields Part I: A Quantitative Comparison of Methods”, *Sol. Phys.* **235**, 161.
- Schrijver, C. J., DeRosa, M. L., Title, A. M., and Metcalf, T. R. 2005, “The Nonpotentiality of Active-Region Coronae and the Dynamics of the Photospheric Magnetic Field”, *ApJ* **628**, 501.
- Sonnerup, B. U. O. 1970, “Magnetic field re-connexion in a highly conducting incompressible fluid”, *J. Plasma Phys.* **4**, 161.
- Sweet, P. A. 1958, “The neutral point theory of solar flares”, in Lehnert, B., editor, *Electromagnetic Phenomena in Cosmical Physics*, pp. 123–134, Cambridge University Press, Cambridge, U.K.
- Tarr, L. A., Longcope, D. W., McKenzie, D. E., and Yoshimura, K. 2014, “Quiescent Reconnection Rate

- Between Emerging Active Regions and Preexisting Field, with Associated Heating: NOAA AR 11112”, *Sol. Phys.* **289**, 3331.
- Testa, P., De Pontieu, B., Allred, J., Carlsson, M., Reale, F., Daw, A., Hansteen, V., Martinez-Sykora, J., Liu, W., DeLuca, E. E., Golub, L., McKillop, S., Reeves, K., Saar, S., Tian, H., Lemen, J., Title, A., Boerner, P., Hurlburt, N., Tarbell, T. D., Wuelser, J. P., Kleint, L., Kankelborg, C., and Jaeggli, S. 2014, “Evidence of nonthermal particles in coronal loops heated impulsively by nanoflares”, *Science* **346**, B315.
- Tsuneta, S. 1996, “Interacting Active Regions in the Solar Corona”, *ApJ* **456**, L63.
- Vasyliunas, V. M. 1975, “Theoretical models of magnetic field line merging I.”, *Rev. Geophys. and Space Phys.* **13**, 303.